Thermal Analysis of Eyring-Powell Hybrid Nanofluid: A Case of Combined Convective Transport and Radiative Heat Flux along Inclined Stretching/Shrinking Sheet

AHLAM ALJABALI[1], ABDUL RAHMAN MOHD KASIM[1,*], ISKANDAR WAINI[2], NAJIYAH SAFWA KHASHI'IE[2], YUSUF OLATUNJI TIJANI[3]
[1]Centre for Mathematical Sciences,
Universiti Malaysia Pahang Al-Sultan Abdullah,
Tun Khalil Yaakob Promenade Highway, 26300 Gambang, Pahang,
MALAYSIA

[2]Faculty of Technology and Industrial Engineering and Manufacturing,
Universiti Teknikal Malaysia Melaka,
Hang Tuah Jaya, Durian Tunggal 76100, Melaka,
MALAYSIA

[3]Department of Mathematics,
Rhodes University, Makhanda,
PO Box 94, Grahamstown 6140,
SOUTH AFRICA

Corresponding Author

Abstract: - Hybrid nanofluids are designed to improve conventional nanofluids' stability and other thermal properties. The present work investigates the flow of combined convective transport and the influence of radiation on the studied flow. A hybrid nanofluid ($Cu-Al_2O_3$/water) flows through a vertically inclined stretching/shrinking sheet. To simplify the governing equations, the deterministic two-variable differential equations (PDEs) are systematically transformed into a system of one-variable differential equations by using appropriate similarity transformations. The bvp4c function of the MATLAB program is also used to solve the simplified mathematical model. The present study investigates and presents in tabular and graphical form the effects of stretching/shrinking surfaces, suction, and volume fraction of the nanoparticles on the velocity and temperature profiles as well as on the engineering quantities. The present results are first validated and confirmed as acceptable before the full calculations are performed. Overall, the results of this study show that the investigated parameters influence the flow characteristics, which can serve as a controlling factor for heat transfer.

Key-Words: - Hybrid nanofluid, Eyring-Powell, mixed convection, inclined stretching/shrinking sheet, dual solution, radiation.

Received: June 2, 2024. Revised: November 13, 2024. Accepted: December 5, 2024. Published: January 24, 2025.

1 Introduction

In engineering and industrial applications, problems related to the performance of energy are crucial. Most fluids immiscible with convection heat, including ethylene glycol, water, and oil, have low thermal conductivity; therefore, heat transfer is limited. Nanofluids are used to increase thermal efficiency. [1], first proposed the concept of nanofluids and defined them as mixtures with dispersed nanometer-sized particles as the base fluid. Considering their importance in thermal and energy efficiency, hybrid nanofluids are widely used in numerical and experimental studies in the field of fluid dynamics. Two different types of nanoparticles are combined to create composite/hybrid nanoparticles: metal oxides (alumina, copper oxide, magnetite, hematite), metals (silver, copper), carbonaceous materials (carbon nanotubes, graphite), or metal carbide. [2], modified the thermophysical properties into the model for single-phase nanofluids. Meanwhile, correlations between the thermophysical properties of hybrid nanofluids were mentioned in [3]. In this study, the natural laminar convection in a sinusoidally corrugated container filled with pure water, Al_2O_3/water nanofluids, and $Cu-Al_2O_3$/water nanofluids was numerically investigated. The container has a separate heat source at the bottom wall. While [4] base their concept of boundary layer flow of nanofluids on the use of Cu and Ag as nanoparticles, [5] investigated the unsteady/steady flow of nanofluids over a moving surface in a continuous external free stream. [6] investigated the effects of water and nanoparticles in porous media, focusing on their influence on Dufour and Soret effects in magnetic flows over a stretched surface. In addition, [7] and [8] performed numerical investigations for hydromagnetic and heat transfer enhancement of the steady boundary layer flow induced by a stretched plate, respectively . Their results suggest that hybrid $Cu-Al_2O_3$/water nanofluids exhibit superior heat transfer rates compared to Cu/water nanofluids. In a related study, [9] discussed the thermal conductivity properties of hybrid nanofluids. The study by [10] explored the heat transfer potential of an alumina-silica-water nanofluid in the context of cold plates for proton electrolyte membrane fuel cells and highlighted its importance for the automotive industry. [11] formulated a model to study the flow and heat transfer characteristics of dusty hybrid nanofluids over an unstable shrinking plate.

Lastly, the features of heat transfer of axisymmetric flow over a nonlinear shrinking/stretching surface induced by hybrid (TiO_2-Ag) nanofluid with radiation impact analytically investigated by [12]. Moreover, in [13], the stability analysis of a radiative-magnetic hybrid nanofluid slip flow due to an exponentially stretching/shrinking permeable sheet with heat generation was attempted, and it was found that the presence of a shrinking surface as well as adequate suction leads to the possibility of achieving two solutions, with only the first solution being stable.

Non-Newtonian fluids have attracted the attention of researchers in recent years as they are widely used in industries such as polymers and rubber. Non-Newtonian fluids such as blood, color, palm oil, mayonnaise, shampoo, and others cannot be modeled using the Navier-Stokes equations that apply to Newtonian fluids due to the complexity of their mathematical models compared to Newtonian fluids. The most common types of non-Newtonian fluids are those described by Powell-Eyring. The analysis of the governing nonlinear differential equations using the Keller box technique was performed by [14] to evaluate the effects of various factors on the flow as well as the boundary layer flow and heat transfer induced by an Eyring-Powell fluid over a stretching surface. [15] applied the collocation method for the Eyring-Powell boundary layer flow of a fluid over a stretched surface in an unconfined area. The study of [16] on the Eyring-Powell fluid using a convective stretching cylinder included thermophoresis, thermal radiation, Brownian motion, and source/sink phenomenon, while [17] and [18] analyzed the convective transport of temperature-dependent viscosity for the single-phase and two-phase flow of Eyring-Powell fluid over a vertically stretched plate. An analytical, numerical and machine learning approach for the Eyring-Powell flow with temperature-dependent viscosity in rotating systems was investigated by [19].

Convection can be categorized into three different types: natural or free convection, forced convection, and mixed convection. The basic concept of natural or free convection is the continuous flow of heat between two surfaces or materials when a strong buoyancy force is present. In forced convection, heat is transferred between the two materials by an external force. The complicated interplay of heat and mass transfer within the unstable boundary layer of a rotating Eyring-Powell fluid was investigated by [20]. [21] studied the effects of boundary layer flow with mixed convection in a double-layered medium on an Eyring-Powell fluid along an inclined, stretched cylinder. In addition, [22] conducted a theoretical study on the steady-state Magnetohydrodynamic (MHD) boundary layer flow of an Eyring-Powell nanofluid over an inclined plane. [23] and [24] examined the dual solutions for the mixed convection flow and heat transfer in a fluid over a stretching/shrinking permeable sheet. In an innovative study, [25] investigated the radiation heat transfer of hybrid nanofluid flow over a stretched surface with Joule effect interaction. [26] applied the shooting technique to analyze the flow of a magnetic Eyring-Powell nanofluid towards a stretching surface and showed dual solutions for convective boundary conditions in the flow of a hybrid nanofluid on a radially shrinking disc under a magnetic field with generated viscous dissipation, as demonstrated by [27]. This work also presented a comprehensive study of lower and higher-branch solutions. More recently, [28] investigated an MHD hybrid nanofluid undergoing mixed convection over a permeable inclined plate, emphasizing the effects of thermal radiation.

Following previous studies, the main strength of this numerical study is to investigate the effects of heat flux due to thermal radiation on the flow of an Eyring-Powell hybrid nanofluid over a non-parallel stretching/shrinking permeable surface using the deterministic nanofluid model introduced by [2]. The model contains fixed-volume fractions of nanoparticles, specifically alumina (Al_2O_3) and copper (Cu), suspended in the base fluid (water) to form a hybrid nanofluid. The analysis is performed using MATLAB and the solver bvp4c by converting the governing equations and boundary conditions into a set of ordinary differential equations through similarity variables. The results, which show the influence of the different parameter values on the physical quantities, are presented graphically and in tabular form. The study concludes with a stability analysis in which dual solutions are discovered for both the stretching and shrinking scenarios. To validate the numerical results, a comparison is also made with the results published in the literature.

2 Mathematical Model

The radiative heat flux effect on mixed convection Eyring-Powell hybrid nanofluid flow is considered a laminar, incompressible, and steady two-dimensional with constant velocity $u_w(x) = \varepsilon x$ in supporting direction or contrary direction to the free-stream velocity, u_∞, where ε is a positive constant induced with analysis thermal. The flow is considered passing toward an inclined stretching/shrinking sheet containing $Cu - Al_2O_3$ nanoparticles with an angle of inclination, α, to the vertical in the $x-$direction and moving at a uniform velocity, where the $x-$ axis determines the upward direction along with the sheet. Meanwhile, its orthogonal orientation to the sheet is assumed by the $y-$axis, as demonstrated in Figure 1 (Appendix). This also involves whether the $x-$ direction is positive or negative and whether the force is either assisting (heated sheet $T_w > T_\infty$) or opposing (cooled sheet $T_w < T_\infty$) the flow. The following assumptions are taken into consideration for the physical model:

- Thermal equilibrium is preserved in the fluid mixtures i.e. base fluid and nanoparticles.
- The influence of nanoparticle aggregation and sedimentation is excluded because it is believed that the nanofluid is stable and that the nanoparticles have a spherical shape.
- For the present, $q_r = -(16\sigma^*/3k^*)(\partial T/\partial y)T_\infty^3$ with the mean absorption, k^*, and Stefan-Boltzmann, σ^* deliberated is used in the energy equation coupled with the flow temperature.
- The surface temperature of the sheet is regarded as $T_w(x) = T_\infty + T_0 x$, where T_0 is a constant and the constant ambient temperature is signified as T_∞.

Furthermore, the formulation of the proposed model is based on the principles of the theory of rate processes. This theory was originally introduced and explained in detail by Eyring and Powell in 1944. To express the governing boundary layer equations for the effect of radiative heat flux on the Eyring-Powell hybrid nanofluid with mixed convection in the Cartesian coordinate system for continuity, momentum, and energy equations are used as described above. A similar fluid model can be found in [17], [7] and [29].

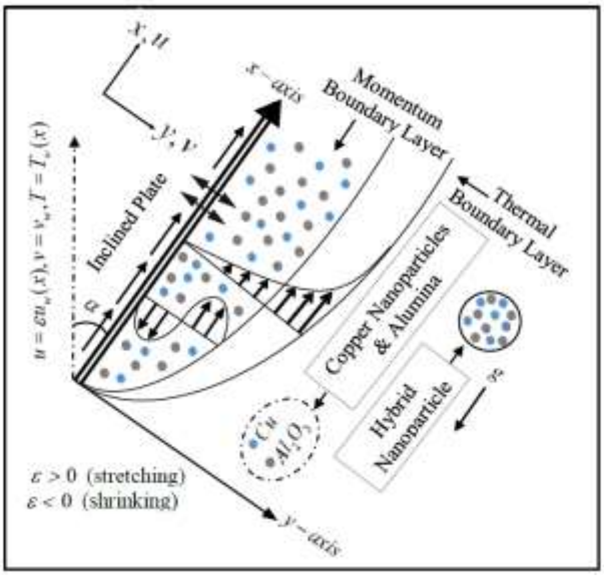

Fig. 1: Geometry of the physical problem

$$\frac{\partial u}{\partial x} + \frac{\partial v}{\partial y} = 0, \tag{1}$$

$$\rho_{hnf}\left(u\frac{\partial u}{\partial x} + v\frac{\partial u}{\partial y}\right) = \mu_{hnf}\frac{\partial^2 u}{\partial y^2} + \frac{1}{\tilde{\beta}c^*}\left(\frac{\partial^2 u}{\partial y^2}\right) - \frac{1}{2\tilde{\beta}c^{*3}}\left(\frac{\partial u}{\partial y}\right)^2\frac{\partial^2 u}{\partial y^2} + (\rho\beta_T)_{hnf}\, g\left(T - T_\infty\right)\cos\alpha, \tag{2}$$

$$(\rho c_p)_{hnf}\left(u\frac{\partial T}{\partial x}+v\frac{\partial T}{\partial y}\right)=\left(k_{hnf}+\frac{16\sigma^* T_\infty^{\ 3}}{3k^*}\right)\frac{\partial^2 T}{\partial y^2}. \quad (3)$$

with the following boundary conditions:

$$u=\varepsilon u_w(x),\ \ v=v_w,\ \ T=T_w(x)\ \text{ at }\ y=0,$$
$$u\to 0,\ \ T\to T_\infty\ \text{ as }\ y\to\infty. \quad (4)$$

where (u,v) are the velocity components in (x,y) directions, respectively, for the hybrid $Cu-Al_2O_3$ /water nanofluid; ρ_{hnf} is the density, where μ_{hnf} is defined as the dynamic viscosity, $(\rho c_p)_{hnf}$ is the heat capacitance, and k_{hnf} is the thermal conductivity. The physical properties of Al_2O_3, Cu and water are given in Table 1 (Appendix), while the thermophysical properties of hybrid and traditional nanofluids are given in Table 2 (Appendix). The dynamic viscosity, density, heat capacity, thermal conductivity, thermal expansion coefficient, and specific heat at constant pressure are represented by $\mu,\rho,(\rho c_p),k,\beta_T$ and c_p, in that order. Subscripts $s1$ and $s2$, respectively, denote the solid components of Al_2O_3 and Cu, whereas ϕ_1 and ϕ_2 represent their corresponding nanoparticle volume fractions. The subscripts hnf; nf; and f, respectively, denote the hybrid nanofluid, nanofluid, and fluid. In addition, according to [14], $\tilde{\beta}=\beta_0 x^{-1}$ and $c^*=c_0 x$ are the fluid parameters of the Eyring-Powell model with constants β_0 and c_0. Besides, $u_w(x)=\varepsilon x$ is the velocity of the stretching/shrinking surface, the parameter ε is for the deformable plate such that $\varepsilon>0$ stands for a stretching plate, $\varepsilon<0$ indicates a shrinking plate, and $\varepsilon=0$ represents a static plate. While $v_w(x)=-S\left(a\upsilon_f\right)^{1/2}$ denotes the constant mass velocity for the surface, S is the suction/injection parameter such that $S>0$ corresponds to the suction effect and $S<0$ refers to the injection (fluid removal) effect.

An appropriate transformation is introduced as follows:

$$\eta=\left(\frac{a}{\nu_f}\right)^{1/2} y,\ \psi=\left(a\nu_f\right)^{1/2} x f(\eta),\ \theta(\eta)=\frac{T-T_\infty}{T_w-T_\infty}. \quad (5)$$

Here, ψ implies stream function defined as $u=\frac{\partial\psi}{\partial y}$ and $v=-\frac{\partial\psi}{\partial x}$, and η is the dimensionless similarity variable, yielding

$$u=axf'(\eta),\ \ v=-\left(a\upsilon_f\right)^{1/2} f(\eta),\ v_w(x)=-S\left(a\upsilon_f\right)^{1/2}. \quad (6)$$

Upon appropriate implementation of (4), (5) and (6) as well as properties listed in Table 1 and Table 2 (Appendix), we obtain:

$$\frac{\mu_{hnf}}{\mu_f}f'''+Mf'''-BM\left(f''\right)^2 f'''$$
$$+\frac{\rho_{hnf}}{\rho_f}\left(ff''-f'^2\right)+\frac{(\rho\beta_T)_{hnf}}{(\rho\beta_T)_f}\lambda\theta\cos\alpha=0, \quad (7)$$

$$\left(\frac{k_{hnf}}{k_f}+\frac{4}{3}R\right)\theta''+\frac{(\rho c_p)_{hnf}}{(\rho c_p)_f}\Pr\left(f\theta'-f'\theta\right)=0. \quad (8)$$

satisfying

$$f(0)=S,\ \ f'(0)=\varepsilon,\ \ \theta(0)=1\ \text{ at }\ \eta=0$$
$$f'(\eta)\to 0,\ \ \theta(\eta)\to 0\ \text{ as }\ \eta\to\infty. \quad (9)$$

where the fluid parameters are M and B, the kinematic viscosity is υ_f, the mixed convection parameter is λ, and the radiation parameter is R.

The equation can be defined as:

$$M=\frac{1}{\mu_f\beta_0 c_0},\ \ B=\frac{a^3}{2c_0^2\upsilon_f},\ \ \upsilon_f=\frac{\mu_f}{\rho_f},$$
$$\lambda=\frac{Gr}{\mathrm{Re}_x^2},\ \ R=\frac{4\sigma^* T_\infty^{\ 3}}{k^* k_f}. \quad (10)$$

where $Gr=g(\beta_T)_f(T_w-T_\infty)x^3/\upsilon_f^2$ is the Grashof number and $\mathrm{Re}_x=ax^2/\upsilon_f$ represents the local Reynold number. Considering that the parameter B is a function of the length scale, x, and that its value changes locally throughout the flow motion, it is important to note that B is the local non-Newtonian parameter based on x. Notably, $\lambda=0$ represents the forced convection flow in the non-buoyant case. In the meantime, $\lambda>0$ denotes the buoyant force that is assisting the flow (upward), while $\lambda<0$ denotes the buoyant force that is opposing the flow (downward) in the case study when the surface is stretching.

The engineering quantities encompass the skin friction coefficient C_f and the local Nusselt number Nu_x, which are designated in the form of:

$$C_f = \frac{\tau_w}{\rho_f u_w^2(x)}, \qquad Nu_x = \frac{x q_w}{k_f\left(T - T_\infty\right)}, \tag{11}$$

where τ_w and q_w are the wall shear stress and heat flux from the plate, respectively, such that:

$$\tau_w = \left(\left(\mu_{hnf} + \frac{1}{\tilde{\beta} c^*} \right) \frac{\partial u}{\partial y} - \frac{1}{6\tilde{\beta}} \left(\frac{1}{c^*} \frac{\partial u}{\partial y} \right)^3 \right)_{y=0},$$
$$q_w = -k_{hnf} \left(\frac{\partial T}{\partial y} \right)_{y=0} + \left(q_r\right)_{y=0}. \tag{12}$$

Leading to:

$$C_f \operatorname{Re}_x^{1/2} = \frac{\mu_{hnf}}{\mu_f} f''(0) + M f''(0) - \frac{B}{3} M f''^3(0),$$
$$Nu_x \operatorname{Re}_x^{-1/2} = -\left(\frac{k_{hnf}}{k_f} + \frac{4}{3} R \right) \theta'(0). \tag{13}$$

where $\operatorname{Re}_x = (a x^2 / \nu_f)$ is the Reynolds number.

3 Stability Analysis

The boundary condition (9) leads to a dual solution for a certain range of physical parameters. Therefore, a stability analysis is performed to determine the stability of the dual solution. The stability analysis begins by considering the non-flow stability, which takes into account the condition of dependence on time. By using the variable (14), it is determined that the continuity equation (1) is satisfied, and then the momentum (2) and energy (3) are transformed into partial differential equations (15) and (16) in the form of η and τ.

$$\psi = \left(a \upsilon_f\right)^{1/2} x f(\eta, \tau), \ \eta = \left(\frac{a}{\upsilon_f} \right)^{1/2} y,$$
$$\theta(\eta, \tau) = \frac{T - T_\infty}{T_w - T_\infty}, \ u = a x \frac{\partial f}{\partial \eta}(\eta, \tau), \tag{14}$$
$$v = -\left(a \upsilon_f\right)^{1/2} f(\eta, \tau).$$

Using the unsteady flow as follows:

$$\frac{\mu_{hnf}}{\mu_f} \frac{\partial^3 f}{\partial \eta^3} + M \frac{\partial^3 f}{\partial \eta^3} - BM \left(\frac{\partial^2 f}{\partial \eta^2} \right)^2 \frac{\partial^3 f}{\partial \eta^3}$$
$$+ \frac{\rho_{hnf}}{\rho_f} \left(f \frac{\partial^2 f}{\partial \eta^2} - \left(\frac{\partial f}{\partial \eta} \right)^2 \right) + \frac{(\rho \beta_T)_{hnf}}{(\rho \beta_T)_f} \lambda \theta \cos\alpha \tag{15}$$
$$- \frac{\rho_{hnf}}{\rho_f} \left(\frac{\partial^2 f}{\partial \eta \partial \tau} \right) = 0,$$

$$\left(\frac{k_{hnf}}{k_f} + \frac{4}{3} R \right) \frac{\partial^2 \theta}{\partial \eta^2} + \frac{(\rho c_p)_{hnf}}{(\rho c_p)_f} \Pr \begin{pmatrix} f \dfrac{\partial \theta}{\partial \eta} - \\ \dfrac{\partial f}{\partial \eta} \theta - \dfrac{\partial \theta}{\partial \tau} \end{pmatrix} = 0. \tag{16}$$

The boundary condition subject to:

$$f(0, \tau) = S, \ \frac{\partial f}{\partial \eta}(0, \tau) = \varepsilon, \ \theta(0, \tau) = 1, \text{ at } \eta = 0$$
$$\frac{\partial f}{\partial \eta}(\eta, \tau) \to 0, \ \theta(\eta, \tau) \to 0 \quad \text{as} \quad \eta \to \infty. \tag{17}$$

The perturbation functions are:

$$f(\eta, \tau) = f_0(\eta) + e^{-\gamma \tau} F(\eta),$$
$$\theta(\eta, \tau) = \theta_0(\eta) + e^{-\gamma \tau} G(\eta). \tag{18}$$

In addition, by using the function (18) the system of equations for the eigenvalue problem (19) and (20) is obtained with the linearized condition used in (21) and solved together with the new boundary condition $F''(0) = 1$.

$$\frac{\mu_{hnf}}{\mu_f} F''' + M F''' - BM f_0''^2 F''' - 2BM f_0'' f_0''' F''$$
$$+ \frac{\rho_{hnf}}{\rho_f} \begin{pmatrix} f_0 F'' - 2 f_0' F' \\ + \gamma F' + f_0'' F \end{pmatrix} + \frac{(\rho \beta_T)_{hnf}}{(\rho \beta_T)_f} \lambda G \cos\alpha = 0, \tag{19}$$

$$\left(\frac{k_{hnf}}{k_f} + \frac{4}{3} R \right) \frac{\partial^2 \theta}{\partial \eta^2} +$$
$$\frac{(\rho c_p)_{hnf}}{(\rho c_p)_f} \Pr \begin{pmatrix} f_0 G' + F \theta_0' \\ -F' \theta_0 + (\gamma - f_0') G \end{pmatrix} = 0. \tag{20}$$

subject to:

$$F(0) = 0, \ F'(0) = 0, \ F''(0) = 1, \ G(0) = 0,$$
$$G(\eta) \to 0 \ \text{ at } \ \eta \to \infty. \tag{21}$$

The stability of the solution is determined by the smallest eigenvalue of γ_1, whereby a negative eigenvalue γ_1 reflects the instability of the flow. A positive eigenvalue γ_1, on the other hand, indicates a stable flow.

4 Validation Procedure

This approach allows the model to achieve similar solutions for both dual scenarios in accordance with equations (7) and (8) and compliance with the boundary conditions listed in equation (9). Numerical analysis of the velocity and temperature profiles is performed to investigate the effects of various physical parameters, including Eyring-Powell fluid properties, stretching/shrinking influences, mixed convection effects and nanoparticle volume fractions. The function bvp4c in MATLAB is used for the numerical resolution of the resulting equations. This solver uses a finite difference method based on the 3-step Lobatto IIIa algorithm to estimate the thickness of the boundary layer and solve the equations effectively. In the study, the influence of these parameters on the skin friction, temperature profiles, velocity fields and heat transfer rates are presented graphically.

The bvp4c method, known for its efficiency in solving flow problems, has been widely applied in numerous studies in this field, taking into account different types and aspects of nanoparticles. Ensuring that the boundary conditions are satisfied is based on the asymptotic behavior of the velocity and temperature profiles shown in Figure 2, Figure 3, Figure 4, Figure 5, Figure 6 and Figure 7 in Appendix. This confirms the methodological accuracy and satisfaction with the physics of the model, which confirms the thickness of the boundary layer considered.

In the current study, a hybrid ($Cu-Al_2O_3$ /water) nanofluid is considered by combining hybrid Cu nanoparticles with 0.1 volume fraction of $Cu-Al_2O_3$ /water to generate the required hybrid nanofluid, similar to [7] and [8]. The base fluid (water) is first treated of Al_2O_3 nanoparticle with 0.1 volume fraction of $\phi_1 = 0.1$ (alumina). Subsequently, Cu (copper) $\phi_2 \le 0.06$ is added along with a variety of solid volume fractions to produce the hybrid nanofluid known as $Cu-Al_2O_3$ /water.

A comparison between the outcomes attained in the present study using the bvp4c method and the exact solution is important to assert that the current model is appropriate and accepted. For this current mathematical model, the non-dimensional physical quantities of the skin friction coefficient and Nusselt number are given as (13). Besides, as evidenced in the literature, the current model can be reduced to the original equation. The following description is provided to demonstrate its correlation to the model.

5 Results and Discussion

The present work analyses the numerical solutions obtained and focuses on the physical interpretation discussion of Eyring-Powell fluid ($Cu-Al_2O_3$/ water) hybrid nanoparticles for the two dissimilar branch solutions obtained (in the form of tables and graphs). The computed results for assorted parameters $M, B, R, \lambda, \varepsilon, \phi_1, \phi_2$ and Pr were performed under RHF. Meanwhile, the computation of $C_f \mathrm{Re}_x^{1/2}$ (skin friction coefficient) and $Nu \mathrm{Re}_x^{-1/2}$ (Nusselt number) is achieved by assigning a set of fixed values of the parameters, which are later computed one by one.

Table 3 (Appendix) illustrates the validation procedures by comparing the values of $C_f \mathrm{Re}_x^{1/2}$ from the results obtained by [14], where ($\phi_1 = \phi_2 = 0$) denotes the regular fluid and $S = \lambda = 0$ with certain values of the physical parameters M and B. Overall, the comparison shows that the algorithms developed in this study are considered reliable and credible as they show close agreement with the reference solutions. This creates confidence in the methodology chosen to solve the problem at hand and increases the probability of novelty and originality of the results obtained, which are not found in the literature. From the present results, it can be deduced that the parameters M and B are the most important determinants of $C_f \mathrm{Re}_x^{1/2}$, reflecting their role in controlling the thermal energy exchange with the environment. However, it should be noted that the presence of M and B leads to different effects, as an increase in M leads to a decrease in $C_f \mathrm{Re}_x^{1/2}$, albeit with opposite effects on the increase in B.

Similarly, the numerical results are validated by a direct comparison with the results documented in the studies of [7], [30] and [31]. The initial branch solution is obtained from the limiting scenarios of the stretching parameter and the absence of radiative heat flux (RHF) for the regular fluid ($\phi_1 = \phi_2 = 0$) in cases where $B = M = S = 0$, $\lambda = 0$ (non-buoyant case), and $\alpha = \pi / 2$. The numerical solutions obtained using the finite difference technique (FDM), Runge-Kutta Fehlberg (RKF) and the bvp4c solution are listed in Table 4 (Appendix) along with the current solution. The high degree of agreement underlines the acceptance of both the present model and its results. Table 5 (Appendix) also shows the effects of $Nu \mathrm{Re}_x^{-1/2}$ the introduction of S and ϕ_2 on the contracting and expanding surface flow scenarios. It is noteworthy that as the volume fraction of copper nanoparticles increases, the value of for the stretching flow increases slightly when $S = 0$.

Analyses of M on $C_f \operatorname{Re}_x^{1/2}$ and $Nu \operatorname{Re}_x^{-1/2}$ profiles for the shrinking surface ($\varepsilon < 0$) when $B = 0.1, \varepsilon = \lambda = -1, \phi_1 = \phi_2 = 0.1, S = 2.2, R = 3, \alpha = \pi / 6$, and $\Pr = 6.2$ are shown in Figure 2 and Figure 3, (Appendix). Evidently, the increase in M contributes to smaller values of $C_f \operatorname{Re}_x^{1/2}$ and greater quantity of $Nu \operatorname{Re}_x^{-1/2}$. Physically, higher values of M act as impediments to the shear-thinning behaviour, diminishing the interaction between the fluid and surfaces and thereby reducing drag forces. Conversely, an increase in ε significantly boosts the values of $C_f \operatorname{Re}_x^{1/2}$. However, when considering $M = 0$, it's observed that the value of $C_f \operatorname{Re}_x^{1/2}$ increases only up to certain levels of ε before it begins to decline. Additionally, the phenomenon of dual solutions for $C_f \operatorname{Re}_x^{1/2}$ and $Nu \operatorname{Re}_x^{-1/2}$ persists only until certain critical values of ε are reached. These critical points are found to be for $\varepsilon_{c1} = -1.2890$, $\varepsilon_{c2} = -1.1799$, and $\varepsilon_{c3} = -1.0861$ for $M = 0, 0.1$ and 0.2, respectively. Beyond these specified critical values, no further solutions are identified.

The effect of ϕ_2 on $f'(\eta)$ and $\theta(\eta)$ when $M = B = \lambda = 0.1, \varepsilon = -1, \phi_1 = 0.01, S = 2.2$, $\alpha = \pi / 6$, $R = 3$ and $\Pr = 6.2$ are given in Figure 4 and Figure 5, (Appendix). Our findings indicate that a higher results in ϕ_2 increased velocity and higher temperatures for the first solution, while for the second solution, fluid velocity decreases as temperatures rise with an increase in ϕ_2. As [7] point out, nanoparticles release energy in the form of heat, which means that a higher concentration of nanoparticles can enhance energy release, increase temperatures and thicken the thermal boundary layer. Furthermore, it is known that hybrid nanoparticles can increase the heat transfer efficiency of fluids through a combined effect of the nanoparticles. Contrary to expectations, this study shows a decrease in heat transfer rates with an increase in the volume fraction of hybrid nanoparticles. This anomaly can be attributed to the significant suction force acting on the shrinking surface and negatively affecting the heat transfer dynamics. Thus, while an increase in the suction parameter generally increases the heat transfer rate, the combined influence of the suction parameter and the volume fraction of the hybrid nanoparticles leads to a decreased heat transfer rate on the shrinking surface when the volume fraction of the hybrid nanoparticles escalates.

The observed dual solutions for velocity ($f'(\eta)$) and temperature distribution ($\theta(\eta)$), highlighted in Figure 6 and Figure 7 (Appendix), are influenced by the buoyancy or mixed convection parameter (λ) when considering the values of, $M = B = \phi_1 = 0.1, \phi_2 = 0.04, S = 2.2$, $R = 3, \alpha = \pi / 6$ and $\Pr = 6.2$. For the first set of solutions, $f'(\eta)$ increases while $\theta(\eta)$ decreases as λ rises. Conversely, for the region where upward buoyant forces dominate ($\lambda > 0$), these parameters show an improvement. The dual solutions present are confirmed by the temperature distributions in Figure 8 (Appendix). It can be clearly seen that both solutions (the first and the second) have developed the temperature profile. Figure 9 (Appendix) displays the relationship between $Nu \operatorname{Re}_x^{-1/2}$ and thermal radiation parameters R and ε. At a constant ε values, a pronounced reduction in $Nu \operatorname{Re}_x^{-1/2}$ with increasing radiation suggests that radiation impedes heat transfer. This phenomenon is particularly evident in the contracting sheet scenario, contributing significantly to the observed outcomes. Moreover, an escalation in R enhances $Nu \operatorname{Re}_x^{-1/2}$, attributed to the energy released by the shrinking sheet which aids in the heat transfer of the fluid. Dual solutions are identified at distinct values of $\varepsilon_c = -1.1799$. Conversely, Figure 10 (Appendix) shows the lowest eigenvalue; here the positive eigenvalue denotes the first solution and the negative eigenvalue the second. This suggests that the first solution behaves consistently and gains confidence over time, while the second option exhibits the exact opposite.

6 Conclusions

This study addressed the problem of steady and thermal analysis of flow over a vertically non-orthogonal stretching/shrinking sheet using the Eyring-Powell hybrid nanofluid. The dynamical equations governing the physics of the problem are solved numerically by employing the bvp4c packages provided in MATLAB. A comparison between the results of this study and those of previous studies for certain cases has been carried out successfully. The impacts of the nanoparticle volume fraction parameter, ϕ_2 (Cu), mass flux parameter, S, mixed convection parameter, λ, stretching/shrinking parameter, ε, fluid parameter, M, radiation parameter, R, on the velocity profile, and temperature, $\theta(\eta)$, local skin friction coefficient, $C_f \operatorname{Re}_x^{1/2}$, and local Nusselt number, $Nu \operatorname{Re}_x^{-1/2}$, are presented and discussed. Overall, the following conclusions are obtained: $Nu \operatorname{Re}_x^{-1/2}$, are presented and discussed. Overall, the following conclusions are obtained:

- A higher value of the Eyring-Powell parameter reduces the viscosity of the fluid, which in turn reduces skin friction and the heat transfer rate.
- The suction strength must be sufficient for the dual solutions to exist.
- The dual solution occurs in a certain range of S, the stretching/shrinking parameter, ε, and mixed convection parameter, λ. In addition, the bifurcation points of the dual solutions occur in the suction region ($S > 0$), shrinking region ($\varepsilon < 0$), and the opposing flow region ($\lambda < 0$).
- Numerical results show an increase in the $C_f \operatorname{Re}_x^{1/2}$ value for the first solution, while the second solution shows a decrease with increasing ϕ_2. In addition, the value of $Nu \operatorname{Re}_x^{-1/2}$ decreases with increasing ϕ_2 for both solutions.
- The rate of heat transfer experiences a rise under significant suction influence. However, when considering both the suction parameter and the hybrid nanoparticle volume fraction simultaneously, an increase in the hybrid nanoparticle volume fraction leads to a reduction in the heat transfer rate on the shrinking surface.
- The values of $C_f \operatorname{Re}_x^{1/2}$ and $Nu \operatorname{Re}_x^{-1/2}$ are higher for the case of flow helping ($\lambda > 0$) compared to the case of flow against ($\lambda < 0$). Besides, it can be observed that the dual solution exists in both regions of flow opposing ($\lambda < 0$) and flow assisting ($\lambda > 0$).
- An increase in the velocity of the hybrid nanofluid is observed when the values of parameters ϕ_2 and λ increase, while the temperature of the hybrid nanofluid increases with increasing values of ϕ_2 but decreases with larger values of λ.
- In the context of a shrinking environment, dual (non-unique) solutions emerge, presenting distinct critical points for varying values of M.
- The velocity distribution $f'(\eta)$ decreases with enhanced value of M (first solution) and shoot upward in the second solution, while $\theta(\eta)$ enhance with the increasing values of R and M.
- A stability analysis was carried out to determine the long-term stability of the dual solution. The results showed that the first solution was stable, and the second solution was unstable.

In the future, this problem may be extended to other geometries, including disc, channel, wedge, and cylinder. In addition, other thermal conditions, such as heat flux and Newtonian heating conditions, can be considered to gain additional insight into fluid behavior.

Acknowledgments:
The authors would like to thank the Ministry of Higher Education Malaysia for providing financial support under the Fundamental Research Grant Scheme (FRGS), FRGS/1/2023/STG06/UMP/02/7 (University reference RDU230124) and Tabung Persidangan Luar Negara (TPLN) from Universiti Malaysia Pahang Al-Sultan Abdullah. An appreciation also goes to Universiti Teknikal Malaysia Melaka and Rhodes University for their encouragement and support.

References:
[1] Choi, S. U., & Eastman, J. A. (1995). *Enhancing thermal conductivity of fluids with nanoparticles* (No. ANL/MSD/CP-84938; CONF-951135-29). Argonne National Lab.(ANL), Argonne, IL (United States).

[2] Tiwari, R. K., & Das, M. K. (2007). Heat transfer augmentation in a two-sided lid-driven differentially heated square cavity utilizing nanofluids. *International Journal of heat and Mass transfer*, *50*(9-10), 2002-2018. https://doi.org/10.1016/j.ijheatmasstransfer.2006.09.034.

[3] Takabi, B., & Salehi, S. (2014). Augmentation of the heat transfer performance of a sinusoidal corrugated enclosure by employing hybrid nanofluid. *Advances in Mechanical Engineering*, *6*,147059. https://doi.org/10.1155/2014/147059.

[4] Vajravelu, K., Prasad, K. V., Lee, J., Lee, C., Pop, I., & Van Gorder, R. A. (2011). Convective heat transfer in the flow of viscous Ag–water and Cu–water nanofluids over a stretching surface. *International Journal of Thermal Sciences*, *50*(5), 843-851. https://doi.org/10.1016/j.ijthermalsci.2011.01.008.

[5] Roşca, N. C., & Pop, I. (2014). Unsteady boundary layer flow of a nanofluid past a moving surface in an external uniform free stream using Buongiorno's model. *Computers & Fluids*, *95*, 49-55. https://doi.org/10.1016/j.compfluid.2014.02.011.

[6] Reddy, P. S., & Chamkha, A. J. (2016). Soret and Dufour effects on MHD convective flow of Al2O3–water and TiO2–water nanofluids past a stretching sheet in porous media with heat generation/absorption. *Advanced Powder Technology*, *27*(4), 1207-1218. https://doi.org/10.1016/j.apt.2016.04.005.

[7] Devi, S. A., & Devi, S. S. U. (2016). Numerical investigation of hydromagnetic hybrid Cu–Al2O3/water nanofluid flow over a permeable stretching sheet with suction. *International Journal of Nonlinear Sciences and Numerical Simulation*, *17*(5), 249-257. https://doi.org/10.1515/ijnsns-2016-0037.

[8] Devi, S. U., & Devi, S. A. (2017). Heat transfer enhancement of Cu–Al2O3/water hybrid nanofluid flow over a stretching sheet. *Journal of the Nigerian Mathematical Society*, *36*(2), 419-433.

[9] Sajid, M. U., & Ali, H. M. (2018). Thermal conductivity of hybrid nanofluids: a critical review. *International Journal of Heat and Mass Transfer*, *126*, 211-234. https://doi.org/10.1016/j.ijheatmasstransfer.2018.05.021.

[10] Idris, M. S., Zakaria, I. A., & Hamzah, W. A. W. (2021). Heat transfer and pressure drop of water based hybrid Al2O3: SiO2 nanofluids in cooling plate of PEMFC. *Journal of Advanced Research in Numerical Heat Transfer*, *4*(1), 1-13, [Online]. https://semarakilmu.com.my/journals/index.php/arnht/article/view/7025 (Accessed Date: October 1, 2024).

[11] Roy, N. C., Hossain, A., & Pop, I. (2022). Flow and heat transfer of MHD dusty hybrid nanofluids over a shrinking sheet. *Chinese Journal of Physics*, *77*, 1342-1356. https://doi.org/10.1016/j.cjph.2021.12.012.

[12] Khan, U., Zaib, A., Ishak, A., Roy, N. C., Bakar, S. A., Muhammad, T., & Yahia, I. S. (2022). Exact solutions for MHD axisymmetric hybrid nanofluid flow and heat transfer over a permeable non-linear radially shrinking/stretching surface with mutual impacts of thermal radiation. *The European Physical Journal Special Topics*, *231*(6), 1195-1204. https://doi.org/10.1140/epjs/s11734-022-00529-2.

[13] Mandal, G., & Pal, D. (2023). Stability analysis of radiative-magnetic hybrid nanofluid slip flow due to an exponentially stretching/shrinking permeable sheet with heat generation. *International Journal of Ambient Energy*, *44*(1), 1349-1360. https://doi.org/10.1080/01430750.2023.2173651.

[14] Javed, T., Ali, N., Abbas, Z., & Sajid, M. (2013). Flow of an Eyring-Powell non-Newtonian fluid over a stretching sheet. *Chemical Engineering Communications*, *200*(3), 327-336. https://doi.org/10.1080/00986445.2012.703151.

[15] Rahimi, J., D. D. Ganji, M. Khaki, & Kh Hosseinzadeh. "Solution of the boundary layer flow of an Eyring-Powell non-Newtonian fluid over a linear stretching sheet by collocation method." *Alexandria Engineering Journal* 56, no. 4 (2017): 621-627. https://doi.org/10.1016/j.aej.2016.11.006.

[16] Hayat, T., Khan, M. I., Waqas, M., & Alsaedi, A. (2017). Effectiveness of magnetic nanoparticles in radiative flow of Eyring-Powell fluid. *Journal of Molecular Liquids*, *231*, 126-133. https://doi.org/10.1016/j.molliq.2017.01.076.

[17] Aljabali, A., Kasim, A. R. M., Arifin, N. S., & Isa, S. M. (2020). Mixed convection of non-Newtonian Eyring Powell fluid with temperature-dependent viscosity over a vertically stretched surface. https://doi.org/10.32604/cmc.2020.012322.

[18] Aljabali, A., Kasim, A. R. M., Arifin, N. S., Isa, S. M., & Ariffin, N. A. N. (2021). Analysis of convective transport of temperature-dependent viscosity for non-Newtonian Erying Powell fluid: A numerical approach. https://doi.org/10.32604/cmc.2020.012334.

[19] Ali, F., Hou, Y., Feng, X., Odeyemi, J. K., Usman, M., & Ahmad, R. (2024). Comparative study of Eyring–Powell fluid flow with temperature-dependent viscosity in roll-rotating systems: An analytic, numeric, and machine learning approach. *Physics of Fluids*, *36*(10). https://doi.org/10.1063/5.0225477

[20] Nadeem, S., & Saleem, S. (2014). Mixed convection flow of Eyring–Powell fluid along

a rotating cone. *Results in Physics*, *4*, 54-62. https://doi.org/10.1016/j.rinp.2014.03.004.

[21] Rehman, K. U., Malik, M. Y., Salahuddin, T., & Naseer, M. (2016). Dual stratified mixed convection flow of Eyring-Powell fluid over an inclined stretching cylinder with heat generation/absorption effect. *AIP Advances*, *6*(7). https://doi.org/10.1063/1.4959587.

[22] Khan, I., Fatima, S., Malik, M. Y., & Salahuddin, T. (2018). Exponentially varying viscosity of magnetohydrodynamic mixed convection Eyring-Powell nanofluid flow over an inclined surface. *Results in physics*, *8*, 1194-1203. https://doi.org/10.1016/j.rinp.2017.12.074.

[23] Lund, L. A., Omar, Z., & Khan, I. (2019). Quadruple solutions of mixed convection flow of magnetohydrodynamic nanofluid over exponentially vertical shrinking and stretching surfaces: Stability analysis. *Computer methods and programs in biomedicine*, *182*, 105044. https://doi.org/10.1016/j.cmpb.2019.105044.

[24] Khashi'ie, N. S., Md Arifin, N., Nazar, R., Hafidzuddin, E. H., Wahi, N., & Pop, I. (2019). Mixed convective flow and heat transfer of a dual stratified micropolar fluid induced by a permeable stretching/shrinking sheet. *Entropy*, *21*(12), 1162. https://doi.org/10.3390/e21121162.

[25] Sharma, R. P., Mishra, S. R., Tinker, S., & Kulshrestha, B. K. (2022). Radiative heat transfer of hybrid nanofluid flow over an expanding surface with the interaction of joule effect. *Journal of Nanofluids*, *11*(5), 745-753. https://doi.org/10.1166/jon.2022.1872.

[26] Duraihem, F. Z., Sher Akbar, N., & Saleem, S. (2023). Mixed convective Eyring-Powell ferro magnetic nanofluid flow suspension towards a stretching surface with buoyancy effects through numerical analysis. *Frontiers in Materials*, *10*, 1109755. https://doi.org/10.3389/fmats.2023.1109755.

[27] Yahaya, R. I., Md Arifin, N., Pop, I., Md Ali, F., & Mohamed Isa, S. S. P. (2023). Dual solutions for MHD hybrid nanofluid stagnation point flow due to a radially shrinking disk with convective boundary condition. *International Journal of Numerical Methods for Heat & Fluid Flow*, *33*(2), 456-476. https://doi.org/10.1108/HFF-05-2022-0301.

[28] Wahid, N. S., Arifin, N. M., Khashi'ie, N. S., & Pop, I. (2023). Mixed convection MHD hybrid nanofluid over a shrinking permeable inclined plate with thermal radiation effect. *Alexandria Engineering Journal*, *66*, 769-783. https://doi.org/10.1016/j.aej.2022.10.075.

[29] Alabdulhadi, S., Waini, I., Ahmed, S. E., & Ishak, A. (2021). Hybrid nanofluid flow and heat transfer past an inclined surface. *Mathematics*, *9*(24), 3176. https://doi.org/10.3390/math9243176.

[30] Khan, W. A., & Pop, I. (2010). Boundary-layer flow of a nanofluid past a stretching sheet. *International journal of heat and mass transfer*, *53*(11-12), 2477-2483. https://doi.org/10.1016/j.ijheatmasstransfer.201 0.01.032.

[31] Waini, I., Ishak, A., & Pop, I. (2019). Hybrid nanofluid flow and heat transfer over a nonlinear permeable stretching/shrinking surface. *International Journal of Numerical Methods for Heat & Fluid Flow*, *29*(9), 3110-3127. https://doi.org/10.1108/HFF-01-2019-0057.

Contribution of Individual Authors to the Creation of a Scientific Article (Ghostwriting Policy)

The authors equally contributed in the present research, at all stages from the formulation of the problem to the final findings and solution.

Sources of Funding for Research Presented in a Scientific Article or Scientific Article Itself

This research was funded by grant FRGS/1/2023/STG06/UMP/02/7 (University reference RDU230124).

Conflict of Interest

The authors have no conflicts of interest to declare.

APPENDIX

Table 1. Thermophysical properties of the base fluid and nanoparticles ([2] and [7])

Thermophysical Properties	Water	Al_2O_3	Cu
$\rho\left(kg/m^3\right)$	997.1	3970	8933
$c_p\left(J/kgK\right)$	4179	765	385
$k\left(W/mK\right)$	0.6130	40	400
$\beta_T\left(K^{-1}\right)$	21×10^{-5}	0.85×10^{-5}	1.67×10^{-5}
$\sigma\left(s/m\right)$	5.5×10^{-6}	35×10^{6}	59.6×10^{6}

Table 2. Thermophysical properties of the hybrid nanofluid ([3], [7])

Properties	Traditional Nanofluid	Hybrid Nanofluid
Thermal Conductivity	$\frac{k_{nf}}{k_f}=\left(\frac{k_s+2k_f-2\phi(k_f-k_s)}{k_s+2k_f+\phi(k_f-k_s)}\right)$	$\frac{k_{hnf}}{k_{bf}}=\left(\frac{\frac{\phi_1 k_{s1}+\phi_2 k_{s2}}{\phi_{hnf}}+2k_{bf}+2(\phi_1 k_{s1}+\phi_2 k_{s2})-2\phi_{hnf}k_{bf}}{\frac{\phi_1 k_{s1}+\phi_2 k_{s2}}{\phi_{hnf}}+2k_{bf}-(\phi_1 k_{s1}+\phi_2 k_{s2})+\phi_{hnf}k_{bf}}\right)$
Dynamic Viscosity	$\frac{\mu_{nf}}{\mu_f}=\frac{1}{(1-\phi)^{2.5}}$	$\frac{\mu_{hnf}}{\mu_f}=\frac{1}{(1-\phi_1)^{2.5}(1-\phi_2)^{2.5}}$
Electrical Conductivity	$\frac{\sigma_{nf}}{\sigma_f}=1+\frac{3(\sigma-1)\phi}{2+\sigma-(\sigma-1)\phi}$, where $\sigma=\frac{\sigma_s}{\sigma_f}$	$\frac{\sigma_{hnf}}{\sigma_{bf}}=\left(\frac{\sigma_{s2}+2\sigma_{bf}-2\phi_2(\sigma_{bf}-\sigma_{s2})}{\sigma_{s2}+2\sigma_{bf}+\phi_2(\sigma_{bf}-\sigma_{s2})}\right)$ where $\frac{\sigma_{bf}}{\sigma_f}=\left(\frac{\sigma_{s1}+2\sigma_f-2\phi_1(\sigma_f-\sigma_{s1})}{\sigma_{s1}+2\sigma_f+\phi_1(\sigma_f-\sigma_{s1})}\right)$
Density	$\rho_{nf}=(1-\phi)\rho_f+\phi\rho_s$	$\rho_{hnf}=(1-\phi_{hnf})\rho_f+\phi_1\rho_{s1}+\phi_2\rho_{s2}$

Table 3. Comparison of value $C_f \operatorname{Re}_x^{1/2}$

	Javed et al. [14]			Present Result		
B	$M=0$	$M=0.2$	$M=0.4$	$M=0$	$M=0.2$	$M=0.4$
0.0	-1.0000	-1.0954	-1.1832	-1.000000	-1.095445	-1.183216
0.2	-1.0000	-1.0924	-1.1784	-1.000000	-1.092445	-1.178431
0.4	-1.0000	-1.0894	-1.1735	-1.000000	-1.089381	-1.173490

Table 4. Comparison of value $-\theta'(0)$

Pr	Khan & Pop [30] FDM solution	Devi & Davi [7] RKF solution	Waini et al. [31] bvp4c solution	Present bvp4c solution
2	0.9113	0.9114	0.9114	0.9116
7	1.8954	1.8954	1.8954	1.8957
20	3.3539	3.3539	3.3539	3.3541

Table 5. $Nu_x \mathrm{Re}_x^{-1/2}$ when $M = B = 0.1, R = 3, \lambda = \phi_1 = 0.01, \alpha = \pi/6, \mathrm{Pr} = 6.2$ and various values of ϕ_2, S, and ε (Stretching / Shrinking Flow)

		$\varepsilon = 1$		$\varepsilon = -1$	
S	ϕ_2	First Solution	Second Solution	First Solution	Second Solution
0	0.10	5.807496	6.022871	-	-
	0.20	5.950035	6.032312	-	-
1.5	0.10	11.933983	11.350308	-	-
	0.20	11.869506	11.286358	-	-
2.5	0.10	17.090635	16.154264	12.115718	7.273882
	0.20	16.847623	15.928535	11.361269	6.768197

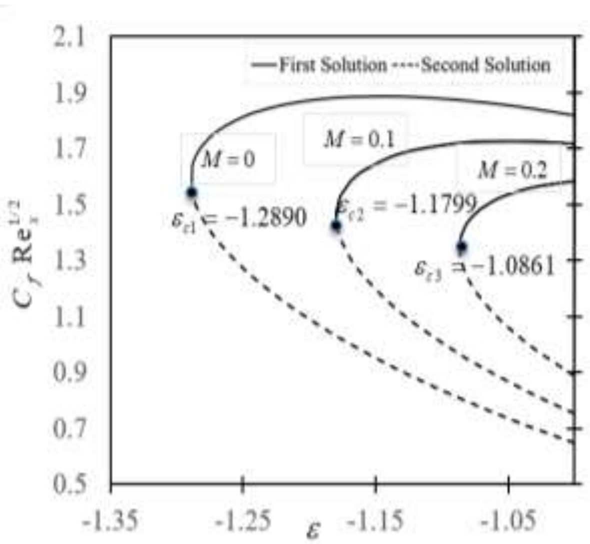

Fig. 2: $C_f \mathrm{Re}_x^{1/2}$ for various M

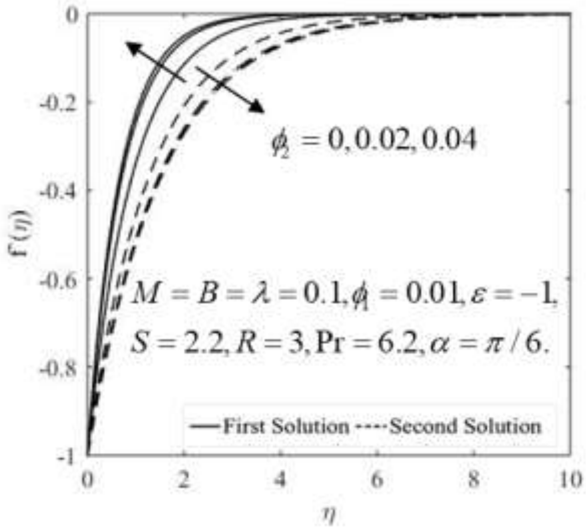

Fig. 4: $f'(\eta)$ for various ϕ_2

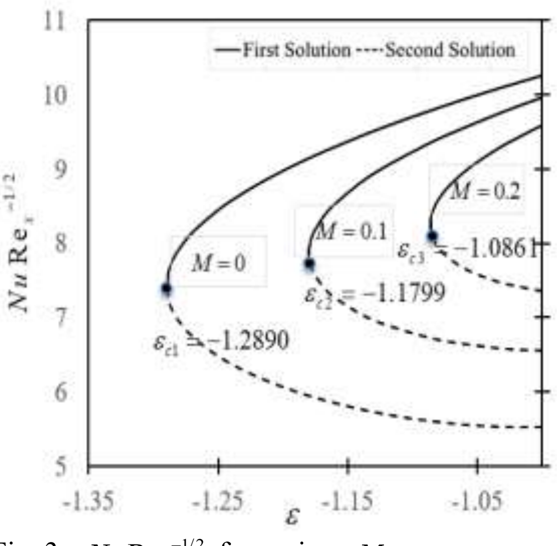

Fig. 3: $Nu \mathrm{Re}_x^{-1/2}$ for various M

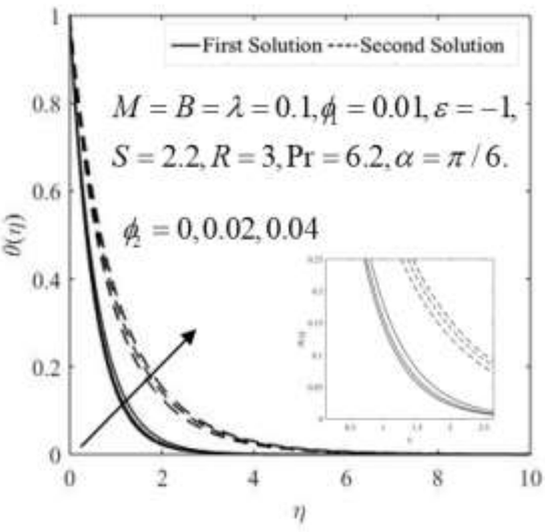

Fig. 5: $\theta(\eta)$ for various ϕ_2

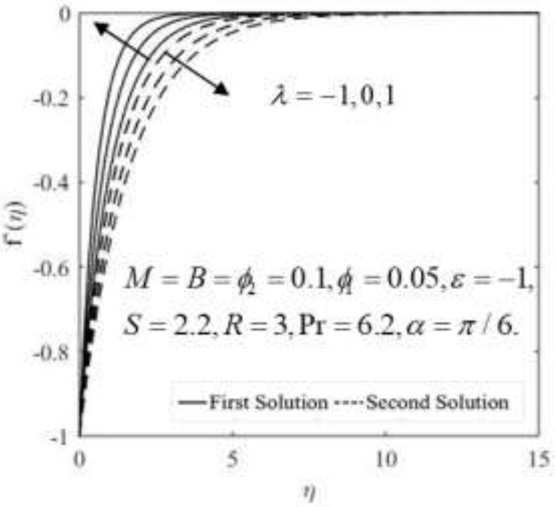

Fig. 6: $f'(\eta)$ for various λ

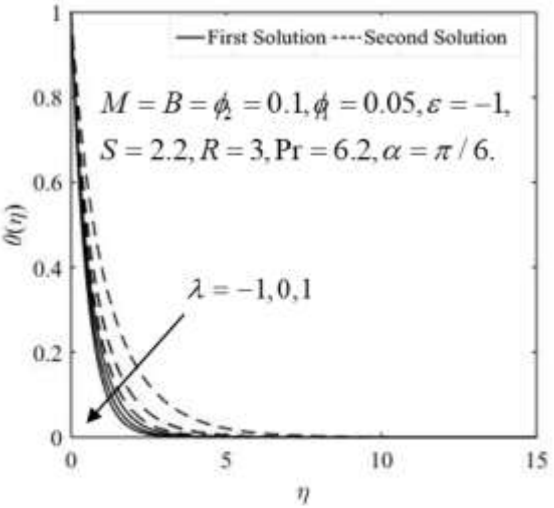

Fig. 7: $\theta(\eta)$ for various λ

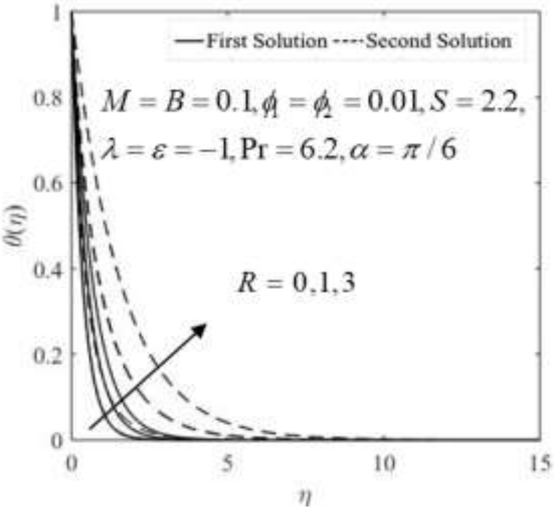

Fig. 8: $\theta(\eta)$ for various R

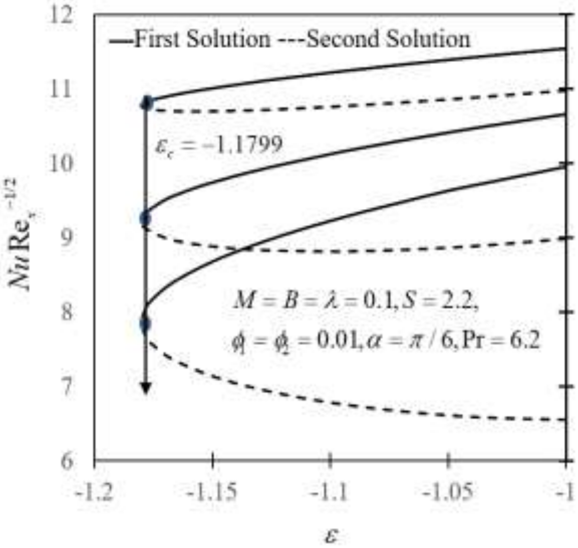

Fig. 9: $Nu \mathrm{Re}_x^{-1/2}$ for various R

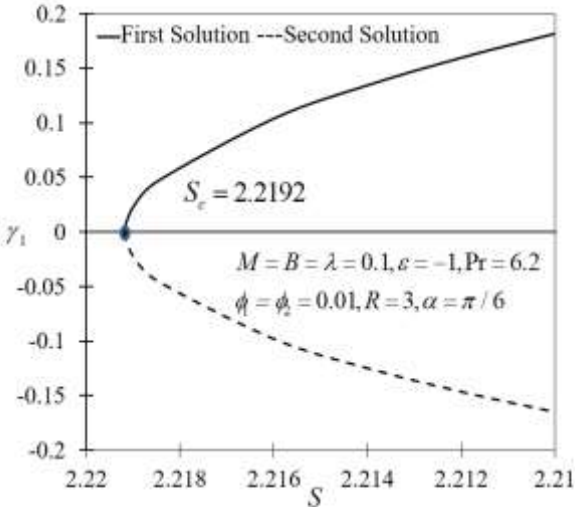

Fig. 10: Smallest eigenvalues (γ_1) of first and second solutions towards S